The Intensity of Ground Motions from Induced Earthquakes with Implications for Damage Potential

Gail M. Atkinson*[1]

ABSTRACT

The damage potential of induced earthquakes is compared to that of natural tectonic events, considering recent instrumental data and felt records from events of M 3.5–5.8 (in which M is the moment magnitude). Ground motions are mutually consistent at close distances (< 30 km) for natural earthquakes in California, induced earthquakes in Oklahoma, and induced earthquakes in western Canada, despite differences in the dominant processes that trigger the events. Recorded peak ground motions may exceed the damage threshold for induced events of M ~ 4.0 within ~ 5 km of the hypocenter; events of M ≥ 4.5 are inferred to have significant damage potential within 5 km and may be damaging to greater distances. Felt and damage effects in Oklahoma, as reported on the U.S. Geological Survey's online "Did You Feel It?" system, show that the damage threshold (modified Mercalli intensity [MMI] = 6) is commonly exceeded for events of M ~ 4.5 at close distances (< 10 km) and that significant damage effects (MMI = 7) are observed for M > 4.8 events within 10 km.

KEY POINTS

- I compared the ground motions and damage potential of induced and natural earthquakes.
- Induced and natural earthquakes have mutually consistent ground motions and damage potential.
- Moderate induced earthquakes have significant damage potential within 10 km.

INTRODUCTION

There is a growing recognition of the potential of earthquakes induced by injection, including wastewater disposal and hydraulic fracture stimulation to produce high-amplitude ground motions that could be damaging to nearby infrastructure (e.g., Atkinson, 2017; Petersen *et al.*, 2017; White *et al.*, 2017; Lee *et al.*, 2019; Lei *et al.*, 2019). Documented examples range from cosmetic damage to vulnerable unreinforced masonry structures for events as small as magnitude 3.4 (Giardini, 2009), to major and/or widespread damage, including personal injury, from events as large as magnitude 5.8 (Yeck *et al.*, 2017; Lee *et al.*, 2019; Lei *et al.*, 2019). Quantitative information on induced ground motions is also growing, enriched by instrumental records from induced events in Oklahoma (Novakovic *et al.*, 2018; Rennolet *et al.*, 2018) and the western Canada sedimentary basin (WCSB) (Novakovic and Atkinson, 2015; Mahani and Kao, 2018; Mahani *et al.*, 2019; Novakovic, 2019). In Oklahoma, there is also a wealth of felt reports from induced events, as archived by the U.S. Geological Survey (USGS) (e.g., Wald *et al.*, 2011; see Data and Resources). The Oklahoma events are mostly related to wastewater injection (Rubinstein and Mahani, 2015), whereas the WCSB records are mostly related to hydraulic fracturing (Atkinson, Eaton, *et al.*, 2016). The growth of quantitative information over the last several years has allowed the development of ground-motion models (GMMs) specific to induced earthquakes (e.g., Novakovic *et al.*, 2018), which supplant earlier GMMs that were based, of necessity, on records from natural events (e.g., Atkinson, 2015; Yenier and Atkinson, 2015a).

In this article, I use the wealth of recent data to compare ground-motion parameters in the moment magnitude (**M**) range from 3½ to 5¾ across three different types of events. The three event types are: (1) earthquakes in California (mostly natural), (2) earthquakes in Oklahoma (mostly induced by wastewater injection), and (3) earthquakes in the WCSB (mostly induced by hydraulic fracturing). The approach taken is to make graphical and statistical comparisons of available data in specified magnitude–distance ranges, rather than to develop new parametric models. The rationale for this approach is to gain insight into broad ground-motion characteristics affecting the

1. Department of Earth Sciences Western University, London, Ontario, Canada

*Corresponding author: gmatkinson@aol.com

Cite this article as Atkinson, G. M. (2020). The Intensity of Ground Motions from Induced Earthquakes with Implications for Damage Potential, *Bull. Seismol. Soc. Am.* **XX**, 1–14, doi: 10.1785/0120190166

potential for damage. Previous studies have compared the felt effects for induced versus natural earthquakes in the central and eastern United States (Hough, 2014; Atkinson *et al.*, 2018) and have proposed models for the amplitudes and attenuation of induced earthquakes based on instrumental data (Atkinson, 2015; Yenier and Atkinson, 2015a; Novakovic *et al.*, 2018). Models have also been proposed to link felt effects to ground motions (Wald *et al.*, 1999; Atkinson and Kaka, 2007; Worden *et al.*, 2012; Atkinson *et al.*, 2014). Previous studies (Hough, 2014; Yenier and Atkinson, 2015a; Huang *et al.*, 2017) have found that induced earthquakes in central and eastern North America (CENA) have lower stress drops on average in comparison to their natural counterparts, though they differ as to the reasons why: Yenier and Atkinson (2015a) showed that this can be interpreted as a focal depth effect, whereas Huang *et al.* (2017) interpreted it as a focal mechanism effect. However, no previous studies have made direct statistical comparisons of ground-motion data for tectonic earthquakes in California versus induced events in CENA. Such comparisons, which are now possible given the quantity of induced seismicity ground-motion data that have been recorded in recent years, can provide new insights into the ground-motion characteristics of induced events. Moreover, the wealth of both instrumental and felt data allows us to map the relationship between recorded ground motions for induced events and their damage effects. This article thus fills a current gap in the literature by analyzing the differences and similarities across event types and showing how they relate to damage potential.

The ground-motion analyses focus on peak ground velocity (PGV) and peak ground acceleration (PGA), which are convenient proxies for the intensity of ground motion at intermediate frequency (PGV) and high frequency (PGA). PGV is a good representation of the strength of ground motion at frequencies of 1–2 Hz, whereas PGA represents the strength of ground motions at 5–10 Hz (e.g., Joyner and Boore, 1982; Newmark and Hall, 1982; Bommer *et al.*, 2000; Bommer and Alarcon, 2005). PGV is considered by many researchers to be a good simple measure of damage potential (e.g., Boatwright *et al.*, 2001; Bommer and Alarcon, 2005; Bommer *et al.*, 2006). I make direct comparisons across event types of PGV and PGA recorded at distances less than 50 km, for earthquakes of $\mathbf{M} \sim 3.5$, 4.0, 4.5, 5.0, and 5.5.

I consider the modified Mercalli intensity (MMI) of events over the same range of magnitude and distance. The intensity of motion can be assessed: (1) using instrumental intensity as calculated from PGV and PGA via a ground motion to intensity conversion equation (GMICE) or (2) using the community decimal intensity (CDI) as reported through the online "Did You Feel It?" system of the USGS (Wald *et al.*, 2011). I show that the intensities obtained from these two information sources (PGV:PGA, CDI) are consistent with each other. Conclusions regarding the damage potential of events in magnitude–distance space are drawn based on observations of the PGV:PGA and MMI of the events.

INSTRUMENTAL GROUND MOTIONS

The damage caused by earthquake shaking will depend on the proximity and vulnerability of structures in addition to the characteristics of the ground motion. Statements such as "the earthquake caused no damage" are not meaningful unless accompanied by an understanding of the structures nearby that might potentially have been damaged. For this reason, I focus on damage potential, recognizing that such potential will not always be realized. The characteristics of ground shaking that influence damage potential are the amplitude, frequency content, and duration of shaking. In very general terms, the damage potential of motions is expected to increase with the amplitude of shaking, the breadth of frequency content (depending on its interaction with structure), and the duration of motion. Earthquake magnitude is often used as a proxy for duration; larger events tend to be more damaging because they last longer, thereby increasing the cumulative distress on a structure responding in the nonlinear range. Distance and site conditions are additional factors that impact duration; duration generally increases with distance and is greater on softer sites.

PGA and PGV recorded on the horizontal component are convenient index parameters for the intensity of shaking at high frequencies (5–10 Hz) and intermediate frequencies (1–2 Hz), respectively. Before the processing of ground-motion records to obtain response spectra became routine, standard response spectra for engineering applications were constructed by scaling PGA by a factor (generally 2–2.5) to represent pseudospectral acceleration (PSA) at high frequencies whereas PGV was scaled by a factor (generally ~1.65) to obtain pseudovelocity at intermediate frequencies (e.g., Joyner and Boore, 1982; Newmark and Hall, 1982; Bommer *et al.*, 2000). Response spectra are useful in engineering seismology because they offer a frequency-specific characterization of motion that can be tied to the predominant period of a structure. Larger structures such as bridges or multistory buildings respond to low-frequency motions (≤3 Hz), whereas small structures (and soil liquefaction effects) are sensitive to high frequencies (≥5 Hz).

As shown in Figure 1, standard response spectra constructed from the average PGA and PGV for induced events of $\mathbf{M} \sim 5$ in Oklahoma at R_{hypo} (hypocentral distance) ~10 km perform reasonably well in characterizing recorded response spectral shapes and average amplitudes of induced events. The standard spectral shape drawn in Figure 1 based on PGV and PGA has not been scaled up by any factor; it is intended only to show overall shape. PGV on Figure 1 is observed to track response spectral amplitudes in the frequency range from approximately 1–10 Hz, although it may be noted that PSA for these records is rising more rapidly than frequency (i.e., slope > 1). This reflects the moderate magnitudes of the records; larger events would be richer in low-frequency content. Because the spectral shape depends on magnitude (and distance) (e.g., Joyner and Boore, 1982), the use of standard spectral shapes was gradually phased out of

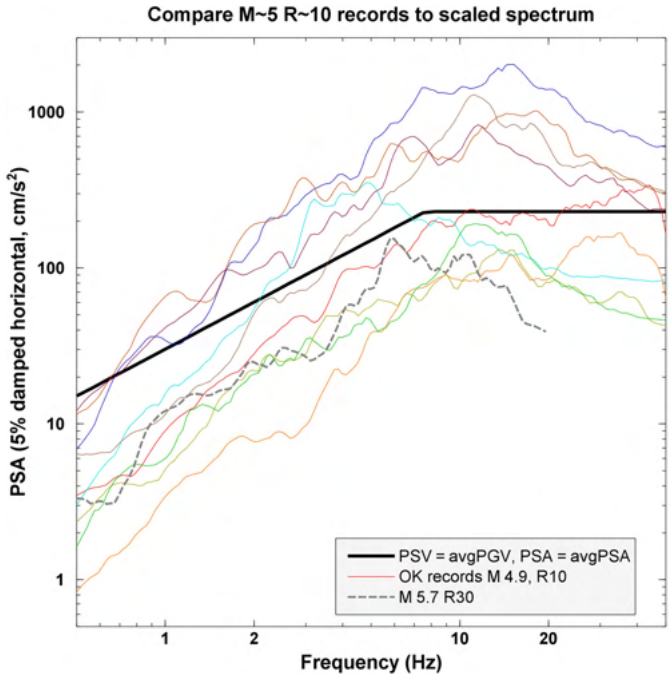

Figure 1. Comparison of a standard response spectral shape constructed by assuming that pseudospectral acceleration (PSA) scales with frequency (f) as ($2\pi f$) peak ground velocity (PGV), to a maximum value of PSA = peak ground acceleration (PGA). The standard spectrum shown is based on the average PGA and PGV values for the plotted records, with no scaling factors applied. The records are the geomean horizontal components for events in Oklahoma of **M** 4.7–5.1 at distances from 3 to 16 km; average **M** 4.9, average R_{hypo} = 10 km, average PGA = 230 cm/s^2, and average PGV = 4.8 cm/s. The color version of this figure is available only in the electronic edition.

engineering practice as the availability of response spectra records made improved approaches feasible. Nevertheless, standard spectra serve to illustrate the overall relationship of PGV and PGA to spectral amplitudes and are thus a guide to their engineering significance. For example, from Figure 1 we could infer that PGV would represent the damage potential of structures with natural vibration frequencies of approximately 0.5–7 Hz, whereas PGA would represent the damage potential of structures with frequencies >5 Hz.

PGV is often used as an index parameter for damage potential because it covers the intermediate frequency range (from ~0.5 to 7 Hz) and is thus a relevant damage measure for a wide range of typical structures (e.g., Bommer and Alarcon, 2005; Bommer *et al.*, 2006). Boatwright *et al.* (2001) showed that PGV was well correlated with the degree of damage to structures in the 1994 Northridge earthquake. PGA is considered by some to be of less physical significance because it is driven by high-frequency pulses of acceleration, which carry too little energy to pose a threat to most structures (Bommer *et al.*, 2006). PGA tends to be well correlated with felt effects at low-intensity levels, whereas PGV is often considered a better measure of higher intensity effects (Wald *et al.*, 1999).

Bommer *et al.* (2006) proposed a limit of PGV = 6 cm/s for damage to weak structures, with a higher limit of PGV = 12 cm/s for severe shaking that would be damaging to many structures; specifically, Bommer *et al.* (2006) predict that damage to adobe houses will commence at a PGV of ~5 cm/s, whereas a PGV of 12 cm/s would damage 80% of houses, with almost 50% experiencing moderate, extensive, or complete damage. This is consistent with the empirical relations of Worden *et al.* (2012) between PGV and MMI for events in California; they find that the median PGV associated with MMI = 6 (the damage threshold) is ~9 cm/s. Studies that include intensity observations from CENA suggest that a somewhat lower PGV, ~6 cm/s, is associated with MMI = 6 (Atkinson and Kaka, 2007); regional differences in the correlation between intensity and ground-motion parameters are not well understood, but may reflect regional differences in either spectral content or vulnerability. PGV has also been used as the criterion for acceptable limits for ground motions from blasting. Westaway and Younger (2014) note that typical international blasting codes and standards impose a limit of 1.5 cm/s to prevent minor cosmetic damage and 6 cm/s for major damage.

PGA is a useful parameter for a range of purposes. PGA may drive felt effects at regional distance, because people are sensitive to acceleration. PGA is also an index parameter (in combination with magnitude) for assessment of the susceptibility to liquefaction (e.g., Seed and Idriss, 1982). Moreover, PGA is a useful damage metric for brittle or high-frequency structures or components, including unreinforced masonry. Worden *et al.* (2012) report that PGA = 110 cm/s^2 is the median PGA associated with MMI = 6, based on observations from California. Atkinson and Kaka (2007), including observations from CENA, report a median PGA of 86 cm/s^2 for MMI = 6. Considering this range, we may conclude that a PGA of ~100 cm/s^2 (10%g) is near the damage threshold for acceleration-sensitive structures. PGA of 5–10 cm/s^2 (or 1%g) is commonly associated with the felt threshold (e.g., Worden *et al.*, 2012). Using the combination of PGA and PGV to predict damage potential is considered superior to using either parameter alone (Worden *et al.*, 2012). In reference to Figure 1, the use of both PGA and PGV would cover a broader spectral range.

It has been suggested that traffic light protocols, which aim to mitigate hazard by changing or ceasing operations when seismicity levels exceed some threshold of concern, should be based on ground motions rather than earthquake magnitudes, because ground motions are more directly tied to consequential effects. The ground-motion threshold for response would depend on the objective. For example, Bommer *et al.* (2006) describe a traffic light protocol for a geothermal project in which thresholds of acceptable ground motion were inferred from regulations concerning tolerable levels of vibration and the vulnerability of the exposed housing stock; the frequency of occurrence of induced events was also taken into consideration. Monitoring of PGV was used to guide decisions

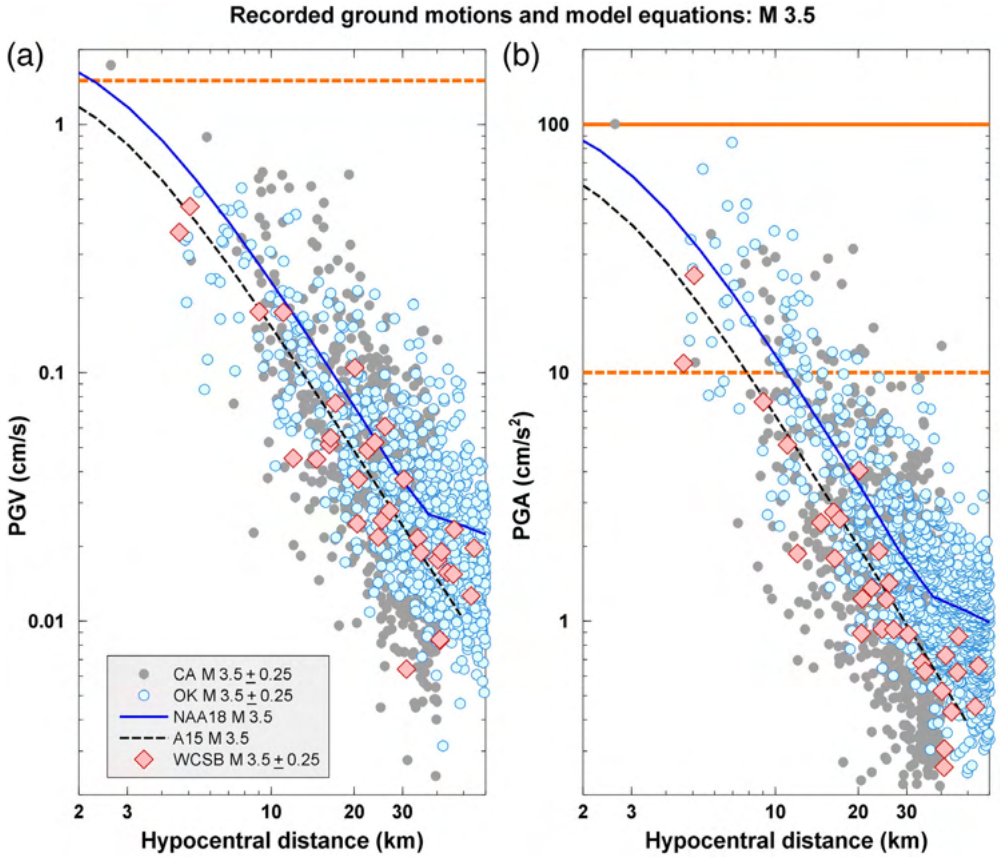

Figure 2. Recorded motions, (a) PGV and (b) PGA, of **M** 3.5 ± 0.25 for California (solid dark circles), Oklahoma (light filled circles), and the western Canada sedimentary basin (WCSB) (diamonds). California and Oklahoma motions are corrected to B/C site condition. California data were used in development of the Atkinson (2015; hereafter, A15) ground-motion model (GMM) (dashed line). Oklahoma data were used in the development of the Novakovic *et al.* (2018; hereafter, NAA18) GMM (solid line). Solid horizontal line shows typical damage thresholds, dashed horizontal line shows felt threshold for PGA, threshold for minor cosmetic damage for PGV. The color version of this figure is available only in the electronic edition.

Comparisons of instrumental motions across event types

I compare recorded PGV and PGA for induced and natural earthquakes of **M** 3.5–5.5 to distances of 50 km. The reference motions are shallow crustal events in California from the Next Generation Attenuation-West2 Project (NGA-W2) database, corrected to a reference B/C site condition (time-averaged shear-wave velocity in the top 30 m of 760 m/s; see Borcherdt, 1994) using the site amplification model of Seyhan and Stewart (2014). This is the dataset that was used by Atkinson (2015; hereafter, A15) in an early GMM for induced events. The California events in the NGA-W2 database are mostly natural in origin, but the functional form of the A15 GMM was constructed to be appropriate for scaling motions from induced moderate-magnitude events at close distances (unlike most of the NGA-W2 GMMs, which were not optimized for this scenario). Oklahoma ground motions, most of which were induced by wastewater injection at depths near 5 km, are those compiled by Novakovic *et al.* (2018; hereafter, NAA18) and used to develop a GMM for induced earthquakes in Oklahoma. The Oklahoma records are also adjusted to B/C, using the station-specific site terms derived in NAA18 by regression. The NAA18 regression was relative to reference sites known to have velocities near 760 m/s. The WCSB ground-motion data, most of which are for events triggered by hydraulic fracturing, are compiled from several recent publications that analyzed such events in Alberta and British Columbia, Canada (see Data and Resources).

The WCSB data have not been corrected to a reference site condition of B/C for two reasons: (1) the site conditions are unknown at most sites and (2) regional studies suggest that typical soil amplification functions for this region are very different than those for California or Oklahoma (e.g., Farrugia *et al.*, 2017; Mahani *et al.*, 2019), making generic corrections problematic. Overall, it is believed that most sites would be classified as National Earthquake Hazards Reduction

regarding the duration and intensity of pumping levels during hydraulic stimulation. The objective of the protocol is a key consideration. A traffic light protocol, whether based on magnitude or ground motion, cannot preclude the occurrence of specified events or ground-motion thresholds (Baisch *et al.*, 2019). Rather, it seeks to reduce the number of follow-on events (which may be bigger or smaller) after a given threshold has been exceeded. In some cases, this may achieve a desired objective—such as reducing the number of felt earthquakes. However, if the objective is to have a high level of confidence that no damaging ground motions will occur, and then the traffic light approach may be ineffective, regardless of whether it is based on magnitude or ground motion. This is because damaging events may not announce themselves with smaller precursory events that would provoke a preventative response action (Baisch *et al.*, 2019). Moreover, the largest and most damaging event in a sequence sometimes occurs during mitigation efforts or after injection has ceased (Yeck *et al.*, 2017; Baisch *et al.*, 2019).

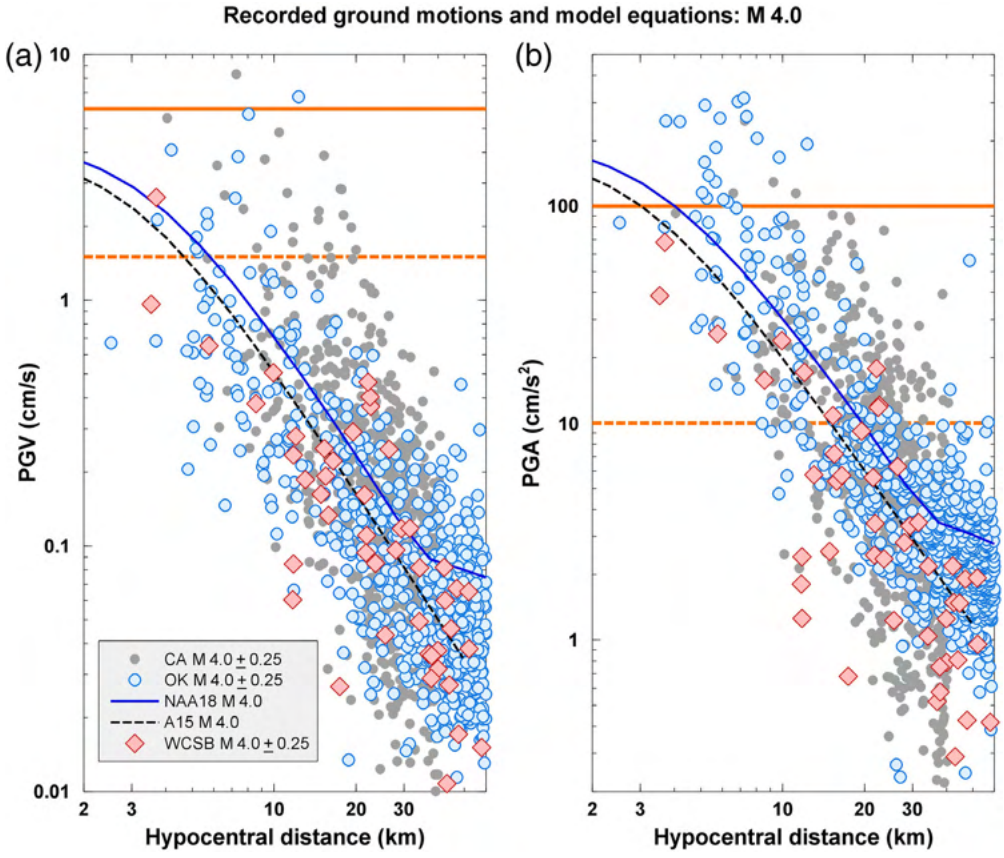

Figure 3. Recorded motions, (a) PGV and (b) PGA, of **M** 4.0 ± 0.25 for California (solid dark circles), Oklahoma (light filled circles), and the WCSB (diamonds). California and Oklahoma motions are corrected to B/C site condition. California data were used in development of the A15 GMM (dashed line). Oklahoma data were used in the development of the NAA18 GMM (solid line). Solid horizontal line shows typical damage thresholds, dashed horizontal line shows felt threshold for PGA, threshold for minor cosmetic damage for PGV. The color version of this figure is available only in the electronic edition.

Program C or D (Borcherdt, 1994; Farrugia *et al.*, 2017), but many sites may have significant site amplification peaks at specific frequencies. Moreover, many of the WCSB seismometers are posthole installations that have been shown to suppress motions at frequencies ≥5 Hz relative to surface installations in the region (J. Holmgren *et al.*, unpublished manuscript, 2020, see Data and Resources). The lack of information on site response for the WCSB data is a significant source of uncertainty in the interpretation of the ground-motion characteristics across event types.

Figures 2–4 compare PGV and PGA for the three event types for **M** 3.5, 4.0, 4.5, respectively, as a function of hypocentral distance. In each case, data are plotted for the specified magnitude ±0.25 units. The Oklahoma data were used in deriving the NAA18 GMM, which is plotted for comparison, whereas the California data were used in deriving the A15 GMM, also plotted. The A15 GMM presented two alternatives to express uncertainty in the near-distance saturation effects. The alt-h version had more near-distance saturation than the other version. Subsequent studies showed that the amount of near-distance saturation in the alt-h variation is more consistent with small-magnitude data in California (Atkinson, Yenier, *et al.*, 2016). The alt-h version of the A15 GMM is therefore used in this study. A15 used data only to 40 km and thus no California data are plotted beyond this distance; the NAA18 GMM used data to hundreds of kilometers, but I focus here on the nearer distances (to 60 km). The A15 GMM has a simple monotonic decay trend, whereas the NAA18 GMM flattens at distances beyond 35 km to model the effects of regional crustal structure on amplitudes. To aid in the interpretation of the figures, several index levels are plotted. Based on the foregoing discussions, PGV = 6 cm/s is plotted as the threshold for damage, with a lower level of 1.5 cm/s to indicate the potential for minor cosmetic damage. For PGA, the felt threshold is plotted at 10 cm/s^2 with the threshold for potentially damaging motions that would be strongly felt plotted at 100 cm/s^2.

Several observations regarding felt effects and potential damage based on recorded PGV and PGA can be made from Figures 2–4. First, PGV values for **M** 3.5–4.5 events in California, Oklahoma, and the WCSB all plot in a similar amplitude range and follow a similar decay trend at distances <30 km. PGA values for WCSB events tend to be noticeably lower than corresponding values for Oklahoma events, and slightly lower than those for California, especially at close distances. The enhanced PGA for Oklahoma relative to California is likely a consequence of the higher stress drop for central and eastern events relative to those in California, for events at the same depth (e.g., Yenier and Atkinson, 2015a,b; Huang *et al.*, 2017). By contrast, the low-PGA values for WCSB events are likely to be related to site effects (including the posthole installations at many sites; J. Holmgren *et al.*, unpublished manuscript, 2020, see Data and Resources). The Oklahoma and California data are both corrected to a site condition of B/C, whereas the WCSB data correspond to a softer site condition. Recent studies suggest that the low-PGA values at close

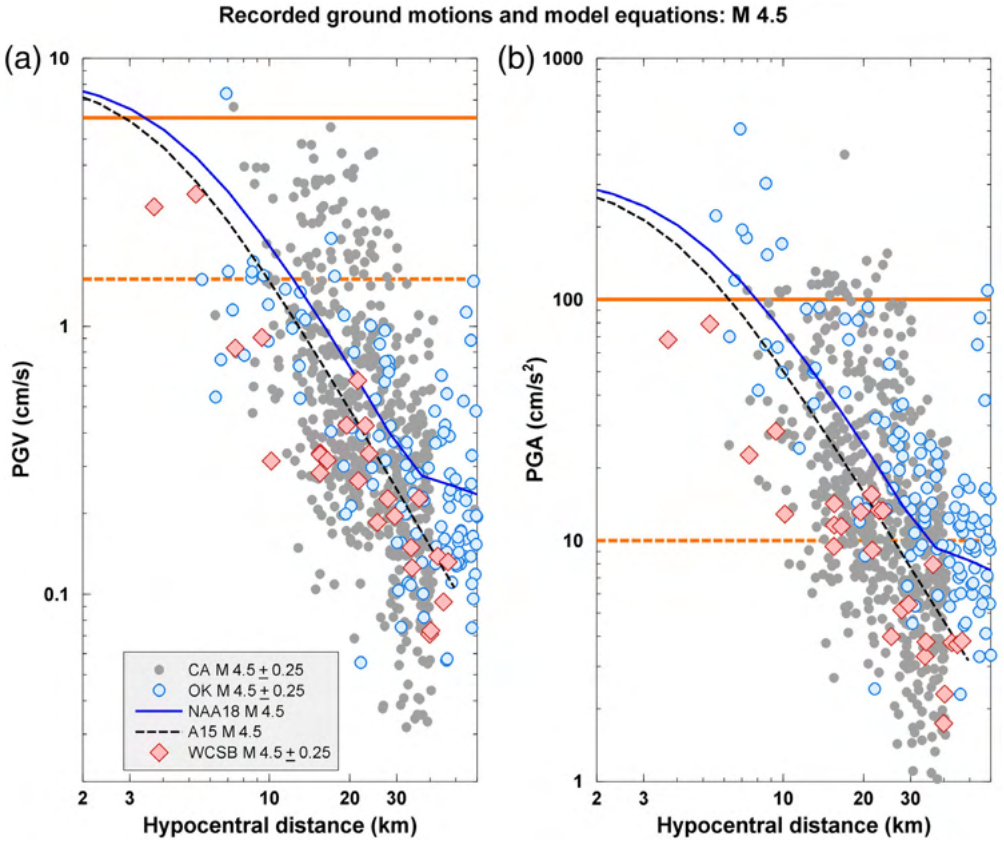

Figure 4. Recorded motions, (a) PGV and (b) PGA, of **M** 4.5 ± 0.25 for California (solid dark circles), Oklahoma (light filled circles), and the WCSB (diamonds). California and Oklahoma motions are corrected to B/C site condition. California data were used in development of the A15 GMM (dashed line). Oklahoma data were used in the development of the NAA18 GMM (solid line). Solid horizontal line shows typical damage thresholds, dashed horizontal line shows felt threshold for PGA, threshold for minor cosmetic damage for PGV. The color version of this figure is available only in the electronic edition.

distances for WCSB events may be due at least, in part, to nonlinear site effects (Mahani *et al.*, 2019). Finally, empirical Green's function analyses that show that the stress drops of WCSB events are at least as large as those observed for events in Oklahoma (Holmgren *et al.*, 2019), supporting the view that the low-observed PGA values in the WCSB dataset are due to site effects.

We can deduce from Figure 2 to 3 that events of **M** ~ 3.5–4.0 would generally be felt by people within 10 km of the hypocenter and might occasionally cause minor damage at close distances. This conclusion is supported by felt and damage reports from induced events at close distances (e.g., Giardini, 2009; Hough, 2014). Figures 2–4 provide insight into why natural events of **M** < 4.5 are not generally considered to have damage potential; natural events are rarely experienced by structures at hypocentral distances less than 8 km due to their focal depth, whereas shorter hypocentral distances (<8 km) are often realized for induced events. Based on Figure 4, events of **M** ~ 4.5 are widely felt within ~30 km and could have significant damage potential within ~5–10 km, depending on the proximity and vulnerability of infrastructure. To place the comparisons of Figures 2–4 on a more quantitative footing, the ground-motion data are recast in the form of residuals relative to the A15(alt-h) GMM. For each observation, the residual is calculated by taking the difference, in log10 units, between the observed PGA or PGV and the value predicted by A15 (alt-h) for the record's magnitude and hypocentral distance. The residuals are binned by distance (in log distance bins) for each 0.5 unit magnitude interval. Figure 5 shows the mean log residual trends along with their 95% confidence limits and standard deviation, for each event type, in magnitude–distance space. The 95% confidence limit portrays our uncertainty on the mean, whereas the standard deviation shows the variability of individual observations relative to the mean. If we consider the statistics of the residuals shown in Figure 5, we reach the following conclusions: (1) PGV residuals for all three event types (California, Oklahoma, and WCSB) are within the 95% confidence limits of zero-mean with respect to the A15(alt-h) GMM, for **M** 3.5–4.5 events, at hypocentral distances from 4 to 30 km; (2) PGA observations are elevated with respect to the A15(alt-h) GMM for Oklahoma events of **M** ≥ 4; and (3) PGA observations are low relative to the A15(alt-h) GMM for WCSB events, especially at close distances (note this may be mostly due to high-frequency site response). These trends are consistent with expectations based on the magnitude and depth dependence of the stress parameter for the CENA and California tectonic environments, according to the empirical GMM models of Yenier and Atkinson (2015a,b). Specifically, the Brune stress parameter for moderate (**M** 4–5) earthquakes has an average value of ~50 bars for: (1) events at ~5 km depth in CENA (Yenier and Atkinson, 2015a, their fig. 9); and (2) events at ~8 km depth in California (Yenier and Atkinson, 2015b, their fig. 8). Deeper CENA events would have a larger stress parameter (Yenier and Atkinson, 2015a).

If damage potential is driven by PGV, I conclude it will be approximately the same across the three event types. To the

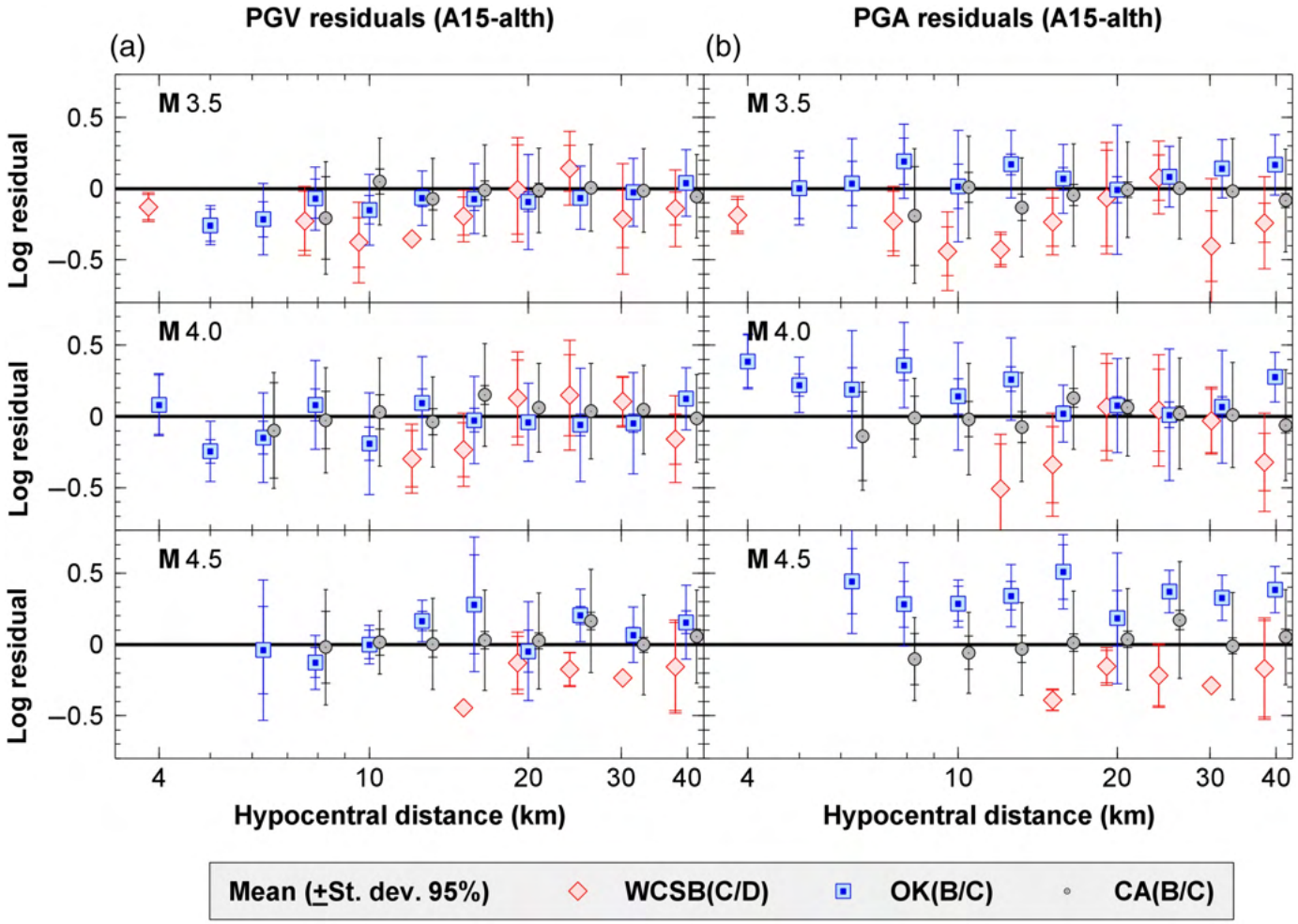

Figure 5. Binned residuals relative to A15(alt-h) GMM for (a) PGV and (b) PGA; plotted for bins with three or more observations. Symbols show mean with 95% confidence limits (inner error bars; if not visible they lie within the symbols) and standard deviation (outer error bars) for natural California events (circles), wastewater-induced events in Oklahoma (squares), and hydraulic fracture-induced events in the WCSB (triangles). Note that California and Oklahoma amplitudes have been adjusted to B/C site condition, whereas WCSB records have not. The color version of this figure is available only in the electronic edition.

extent that damage potential may also be influenced by PGA, it may be higher for $\mathbf{M} > 4$ induced events in Oklahoma in comparison to natural events in California.

The largest events from hydraulic fracturing in the WCSB are **M** 4.6, so we rely on observations from events in Oklahoma and California to infer felt effects and damage potential for larger events. These observations, provided on Figures 6 and 7, suggest that induced events of $\mathbf{M} \sim 5$ have significant damage potential to a distance of ~10 km, whereas events of $\mathbf{M} \sim 5.5$ would have damage potential to a distance of ~20 km. No comparison of binned residuals is attempted for $\mathbf{M} > 5$ events due to the paucity of Oklahoma and WCSB data at close distances. The degree of damage depends on how strong the motions are relative to median levels, as well as the vulnerability of proximate structures. The random variability of ground-motion amplitudes is a significant factor to consider in assessing damage potential based on a scenario magnitude and distance, because observations that are a factor of two or three times the median levels are fairly common (i.e., a factor of two is approximately one standard deviation).

FELT INTENSITIES OF INDUCED EVENTS

The previous section used instrumental ground-motion data to infer that natural events in California, wastewater-induced events in Oklahoma, and hydraulic-fracture induced events in the WCSB all have similar damage potential (for events of **M** 3.5–5.5 within 50 km). Ground-motion data suggest that the threshold for light damage may be crossed for events of: $\mathbf{M} \sim 3\frac{1}{2}$ within 3 km (hypocentral distance), $\mathbf{M} \sim 4$ within ~5 km, $\mathbf{M} \sim 4\frac{1}{2}$ within ~10 km, and **M** 5+ within ~30 km (considering the median plus a standard deviation). To what extent can we validate these inferences with observations of damage effects? In addition to the instrumental data gathered in recent years, there has been a wealth of intensity data gathered by the online intensity reporting program of the USGS (often referred to as "Did You Feel It?") (Wald *et al.*, 2011). Respondents answer a series of questions regarding the shaking they experienced and its effects on the built environment

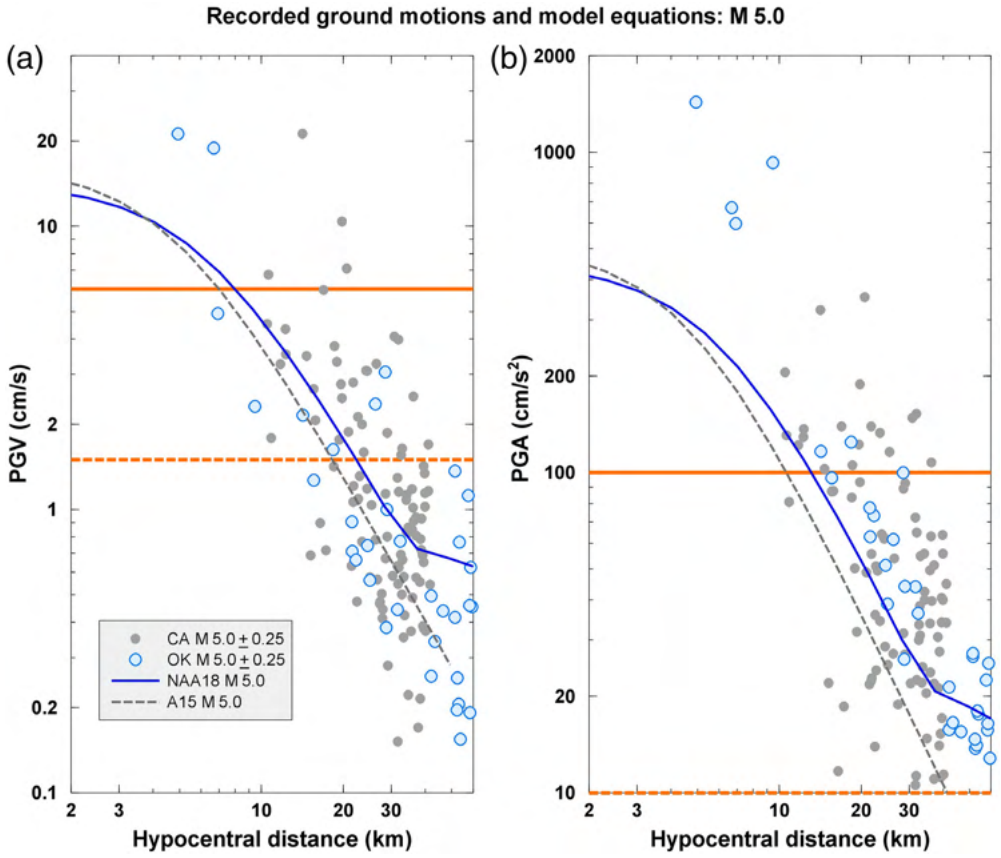

Figure 6. Recorded motions, (a) PGV and (b) PGA, of **M** 5.0 ± 0.25 for California (solid dark circles) and Oklahoma (light filled circles), corrected to B/C site condition. California data were used in development of the A15 GMM (dashed line). Oklahoma data were used in the development of the NAA18 GMM (solid line). Solid horizontal line shows typical damage thresholds, dashed horizontal line shows felt threshold for PGA, threshold for minor cosmetic damage for PGV. The color version of this figure is available only in the electronic edition.

around them. The answers are aggregated in geographic grid cells 1 km in dimension to produce a consensus-based CDI that is equivalent to the MMI (Wald *et al.*, 2011). The CDI is thus a survey-based measure of felt and damage effects that is semiqualitative in nature. In this section, I examine the CDI database of Atkinson *et al.* (2018) for induced earthquakes in Oklahoma; the database has been updated to include significant events of the last two years (see Data and Resources). The CDI database represents ~80, 000 responses from over 400 earthquakes of **M** ≥ 3.5, covering the intensity range from 2 to 8. An intensity of 2 is the lower end of the felt threshold; events are widely felt for intensity levels 3 and above. Intensity 6 is the damage threshold; it corresponds to strong shaking with slight possible damage effects such as fallen plaster. For intensity 7, damage may be considerable in poorly built structures, but slight in buildings of good design and construction. An intensity of 8 corresponds to severe shaking with significant damage to ordinary substantial structures, including partial collapse, and possible foundation failures due to soil effects such as liquefaction; damage to vulnerable structures may be severe (U.S. Geological Survey, 1989; Dewey *et al.*, 2002).

The power and value of the CDI data are that it comprises a vast compendium of observations, including abundant reports at close distances, for which instrumental records are sparse. A drawback of CDI data is its high variability and semiquantitative nature. Moreover, it is a dynamic measure, designed to be updated as new reports arrive and are postprocessed (see Wald *et al.*, 2011). The high variability of CDI data can be mitigated by examining median intensity in distance bins, which reveals underlying average trends that are stable and robust. Previous studies have shown that, on average, CDI is very well correlated with instrumental ground-motion measures, particularly PGV and PGA (Atkinson and Wald, 2007). It has also been shown that a regionally appropriate GMM for PGV and/or PGA can be combined with an empirical equation that correlates MMI with PGV or PGA (known as a GMICE), to predict the expected intensity as a function of magnitude and distance (e.g., Atkinson *et al.*, 2014, 2018). In other words, we can transform a GMM for PGV or PGA into a GMM for MMI. In this study, I use the Atkinson and Kaka (2007) GMICE for this purpose, because it includes data from CENA, in addition to California data, and has been shown to be most applicable for induced events in Oklahoma (White *et al.*, 2017). I calculate the inferred MMI from PGV and PGA, equally weighted.

Figures 8–10 plot observed MMI (as measured by CDI) for **M** ~ 3.5, 4.0, and 4.5 in Oklahoma in distance bins, along with median values and standard deviation; fractiles of the observed values are also shown. (The compiled intensity dataset of Atkinson *et al.*, 2018, does not contain events of **M** < 3.5, and, therefore, the GMMs for the **M** ~ 3.5 data are plotted at **M** 3.6, corresponding to observations from **M** 3.5 to 3.7.) The very wide scatter of MMI observations is apparent, with 1 standard deviation being about 1 MMI unit. The band from

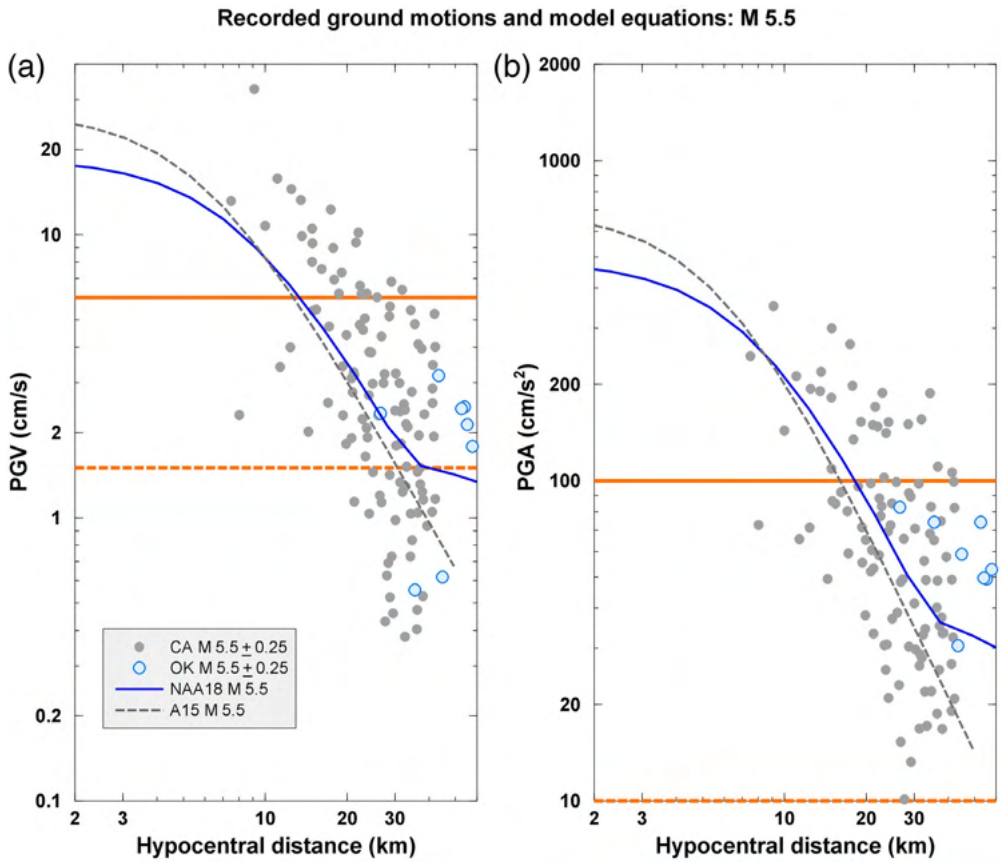

Figure 7. Recorded motions, (a) PGV and (b) PGA, of **M** 5.5 ± 0.25 for California (solid dark circles) and Oklahoma (light filled circles), corrected to B/C site condition. California data were used in development of the A15 GMM (dashed line). Oklahoma data were used in the development of the NAA18 GMM (solid line). Solid horizontal line shows typical damage thresholds, dashed horizontal line shows felt threshold for PGA, threshold for minor cosmetic damage for PGV. The color version of this figure is available only in the electronic edition.

the 5th to the 95th percentile of observations often stretches over four intensity units. Part of the reason for the high variability is that many of the grid cells are based on a single response and are thus not robust intensity measures. Ideally, we would consider only those grid cells having at least three respondents, but this restriction would result in dramatically culling the observational database in many important magnitude–distance ranges (see Figs. 8–10). Tests of the effect of implementing such a data culling (i.e., considering only cells with at least three respondents) indicated that the median statistics are stable. The effect of restricting the statistics to cells with multiple respondents is primarily to narrow the range of the 5th to 95th percentile, such that it would more nearly correspond to the plotted range for the 25th to 75th percentile (i.e., as obtained when considering all cells). I, therefore, consider the plotted 25th to 75th percentiles to be a robust indicator of uncertainty on the true median for the MMI observations.

The MMI observations in Figures 8–10 are compared to expectations based on the GMMs of NAA18 and A15 for PGV and PGA, respectively, in which PGV and PGA are each converted to MMI using the Atkinson and Kaka (2007; hereafter, AK07) GMICE, and then the average of the two values is taken. The conversion depends mainly on the amplitude of PGV:PGA, but also has magnitude and distance as dependent variables, thus accounting indirectly for duration. The GMMs are for B/C but the intensity observations correspond to a wide range of site conditions, most of which are likely softer than B/C. For example, Allen *et al.* (2012) infer that the predominant site class for MMI observations in active tectonic regions is C/D. I, therefore, also plot expected MMI values obtained by converting the NAA18 and A15 GMMs to equivalent values for a soft site (200 m/s), assuming the site amplification model of Seyhan and Stewart (2014). The rationale in plotting the intensity conversions for site conditions that are both firmer than average (B/C) and softer than average (D) is to portray the expected range in observed intensity over a wide range of site conditions. We might expect that higher-than-average intensities would correspond to softer-than-average site conditions.

It is interesting to note in Figures 8–10 that the predicted decay trends for intensity have a somewhat complex shape due to the interplay of distance dependencies in the GMMs and GMICE. Overall, the median values of the observed intensities are consistent with expectations based on the GMMs for B/C site conditions, whereas the median plus standard deviation intensity values are consistent with the GMMs amplified to soft soil (200 m/s) conditions. Overall, the observed MMI values from Oklahoma agree well with those inferred from GMMs for PGV:PGA, which supports the contention that PGV:PGA is a good predictor of damage potential and felt effects.

I converted the WCSB PGV records to inferred MMI using the AK07 GMICE and included these inferred intensities in Figures 8–10. The use of PGV as a proxy for MMI is necessary because actual MMI observations from WCSB events are not available for comparison, due to the sparse population density

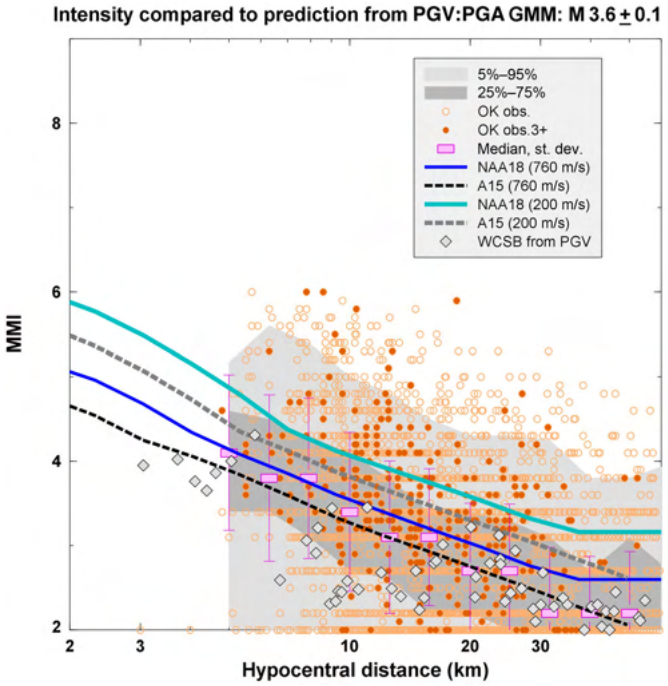

Figure 8. Modified Mercalli intensity (MMI) observations (in 1 km geocoded cells) for Oklahoma events of **M** 3.5–3.7 (circles); site conditions of MMI observations are variable. Darker symbols highlight the cells that are more reliable, having a community decimal intensity (CDI) that is based on at least three respondents. Squares with error bars show median and standard deviation, including all cells in the distance bin; no median is plotted if there are fewer than three CDI values in the distance bin. Shading shows 5th to 95th (light) and 25th to 75th (dark) percentiles of the observations (all cells). Prediction based on PGV:PGA from GMMs of NAA18 (solid line) and A15 (dashed line) with Atkinson and Kaka (2007; hereafter, AK07) ground motion to intensity conversion equation (GMICE) are shown, with lower (thinner) lines being predictions for B/C site condition and upper (thicker) lines being for D site condition. Values of PGV for WCSB events of **M** 3.5 ± 0.25 (diamonds) converted to MMI using AK07 GMICE also shown. The color version of this figure is available only in the electronic edition.

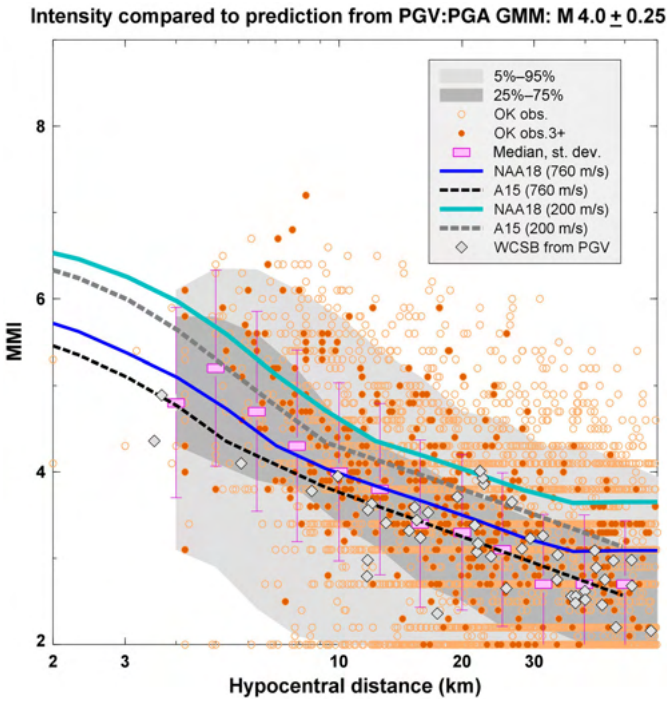

Figure 9. MMI observations (in 1 km geocoded cells) for Oklahoma events of **M** 4.0 ± 0.25 (circles); site conditions of MMI observations are variable. Darker symbols highlight the cells that are more reliable, having a CDI that is based on at least three respondents. Squares with error bars show median and standard deviation, including all cells in the distance bin; no median is plotted, if there are fewer than three CDI values in the distance bin. Shading shows 5th to 95th (light) and 25th to 75th (dark) percentiles of the observations (all cells). Prediction based on PGV:PGA from GMMs of NAA18 (solid line) and A15 (dashed line) with AK07 GMICE are shown, with lower (thinner) lines being predictions for B/C site condition and upper (thicker) lines being for D site condition. Values of PGV for WCSB events of **M** 4.0 ± 0.25 (diamonds) converted to MMI using AK07 GMICE also shown. The color version of this figure is available only in the electronic edition.

in the area where events are occurring combined with the lack of a systematic approach to collect such data. For the WCSB events, PGV is considered a better proxy measure of intensity than PGA because the WCSB events feature low-PGA values that are attributed to regional site response effects, including the widespread use of seismometer installations in postholes, which have been shown to damp amplitudes for frequencies above 5 Hz and PGA (J. Holmgren *et al.*, unpublished manuscript, 2020, see Data and Resources). Further investigation is needed to better understand the causes and implications of the low-observed PGA values for WCSB events.

Overall, the inferred intensities for WCSB events lie in the lower half of the observed range of observed MMI for Oklahoma; they would be most consistent with predictions based on the GMM and GMICE assuming B/C site conditions, even though the site conditions are believed to be softer than B/C. The inferred intensity of WCSB motions appears to be weak near 10 km for **M** 3.5 and weak for **M** 4.5 at <10 km, relative to observations in Oklahoma. These observations may not be statistically significant, because the data are too sparse to provide robust average values; for example, all the **M** 4.5 data at close distances for the WCSB come from a single event (the 2018 Fort St. John event). Moreover, the WCSB amplitudes may be influenced by significant nonlinear site response.

Figures 11 and 12 plot MMI observations for Oklahoma for **M** 5.0 and 5.5, in comparison to predictions based on GMMs for PGV:PGA and the AK07 GMICE. The scatter of observations is large due to the paucity of cells having multiple observations, especially at close distances. The observations suggest that MMI ranges from 4 to 7 for events of **M** ~ 5 at distances <15 km, implying a broad range of potential damage effects from very minor to very significant. For **M** ~ 5.5, observed MMI within 20 km ranges from 4 to 8. These conclusions are consistent with damage reports from induced events in

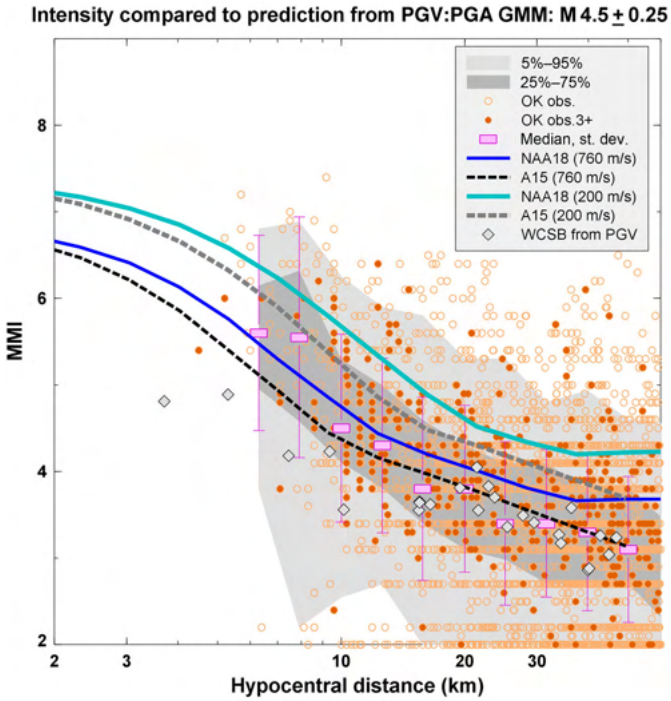

Figure 10. MMI observations (in 1 km geocoded cells) for Oklahoma events of **M** 4.5 ± 0.25 (circles); site conditions of MMI observations are variable. Darker symbols highlight the cells that are more reliable, having a CDI that is based on at least three respondents. Squares with error bars show median and standard deviation, including all cells in the distance bin; no median is plotted, if there are fewer than three CDI values in the distance bin. Shading shows 5th to 95th (light) and 25th to 75th (dark) percentiles of the observations (all cells). Prediction based on PGV:PGA from GMMs of NAA18 (solid line) and A15 (dashed line) with AK07 GMICE are shown, with lower (thinner) lines being predictions for B/C site condition and upper (thicker) lines being for D site condition. Values of PGV for WCSB events of **M** 4.5 ± 0.25 (diamonds) converted to MMI using AK07 GMICE also shown. The color version of this figure is available only in the electronic edition.

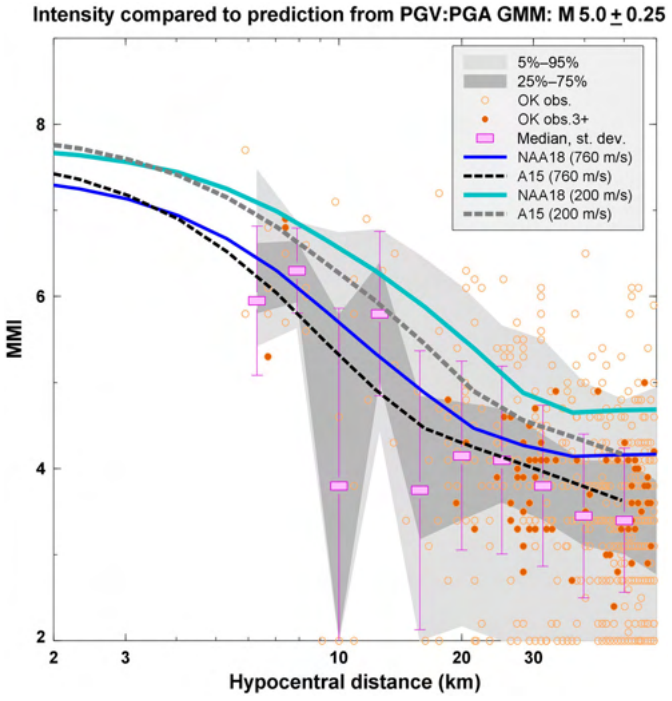

Figure 11. MMI observations (in 1 km geocoded cells) for Oklahoma events of **M** 5.0 ± 0.25 (small solid circles); site conditions of MMI observations are variable. Darker symbols highlight the cells that are more reliable, having a CDI that is based on at least three respondents. Squares with error bars show median and standard deviation, including all cells in the distance bin; no median is plotted if there are fewer than three CDI values in the distance bin. Shading shows 5th to 95th (light) and 25th to 75th (dark) percentiles of the observations (all cells). Prediction based on PGV:PGA from GMMs of NAA18 (solid line) and A15 (dashed line) with AK07 GMICE are shown, with lower (thinner) lines being predictions for B/C site condition and upper (thicker) lines being for D site condition. The color version of this figure is available only in the electronic edition.

Oklahoma and other global settings. For example, Yeck *et al.* (2017) report intensities of 6–8 from the largest Oklahoma events, including damage to brick buildings, and soil liquefaction and slumping in the epicentral region. A 2017 **M** 5.5 event in Korea induced by hydraulic fracturing in a geothermal project, injured 135 people and caused more than $75 million in direct damages to more than 57,000 structures (Lee *et al.*, 2019). In 2018, an **M** 5.7 event induced by hydraulic fracturing in a shale gas development in the Sichuan basin in China caused the collapse of nine houses, extensive damage to 390 houses, and large-scale landslides and rock collapses, with 19 people being injured (Lei *et al.*, 2019). Lei *et al.* (2019) noted that extensive damage to >500 houses was reported in an earlier 2017 **M** 4.7 event in the same region.

In this study, no direct comparisons have been made of CDI-based intensities from natural and induced events. Rather, the relative intensities of different event types are assessed based on specified GMMs converted to intensity via a GMICE; the use of this approach is supported by agreement of predicted intensities with observations in Oklahoma. Previous work by Hough (2014) has shown that natural and induced events in the central and eastern United States have similar intensities at close distances. Hough (2014) reports lower intensities for induced versus natural events within the central United States at larger distances, which she attributes to lower stress for induced versus natural events. Her findings are generally consistent with the results of this study: my comparison set for natural events is drawn from California, which tend to have lower stress drops than eastern events for the same focal depth (e.g., Yenier and Atkinson, 2015a,b).

CONCLUSIONS

1. The ground-motion amplitudes for moderate events (**M** 3.5–5.5) are mutually consistent for natural earthquakes in California, induced earthquakes in Oklahoma and induced earthquakes in western Canada at close distances (<40 km), despite differences in the dominant processes that trigger the

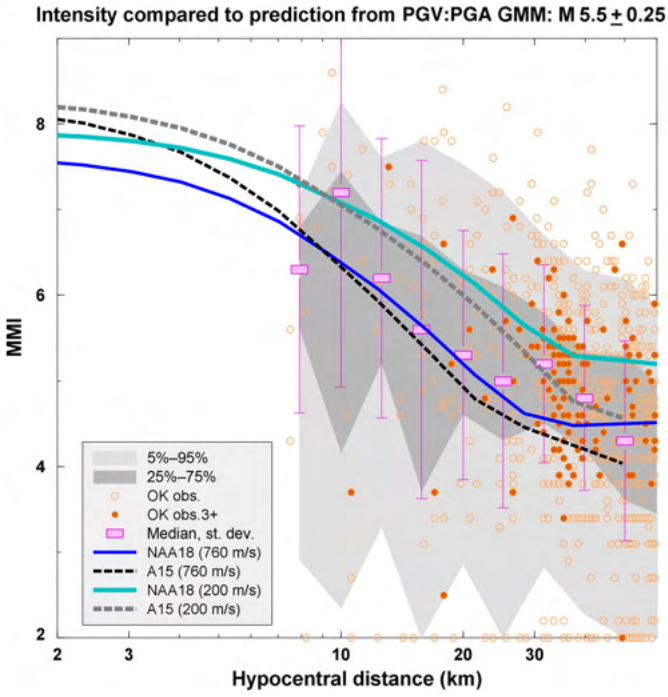

Figure 12. MMI observations (in 1 km geocoded cells) for Oklahoma events of **M** 5.5 ± 0.25 (small solid circles); site conditions of MMI observations are variable. Darker symbols highlight the cells that are more reliable, having a CDI that is based on at least three respondents. Squares with error bars show median and standard deviation, including all cells in the distance bin; no median is plotted if there are fewer than three CDI values in the distance bin. Shading shows 5th to 95th (light) and 25th to 75th (dark) percentiles of the observations (all cells). Prediction based on PGV:PGA from GMMs of NAA18 (solid line) and A15 (dashed line) with AK07 GMICE are shown, with lower (thinner) lines being predictions for B/C site condition and upper (thicker) lines being for D site condition. The color version of this figure is available only in the electronic edition.

events (i.e., natural tectonic processes, wastewater injection, and hydraulic fracturing, respectively).

2. Based on recorded ground motions (PGV:PGA), induced events have damage potential within 5 km of the hypocenter for **M** ~ 4.0 and within 10 km for **M** ~ 4.5; smaller events (**M** ~ 3.5) events may cause minor damage at very close distances (<5 km), whereas larger events of **M** ~ 5.0–5.5 may be damaging to greater distances (10–20 km). These conclusions are consistent with international examples of damage from small-to-moderate events (e.g., Giardini, 2009; Lee *et al.*, 2019; Lei *et al.*, 2019).
3. Intensity observations from induced earthquakes in Oklahoma show that events of **M** ~ 4.5 at close distances (<10 km) frequently cross the damage threshold (MMI 6) and sometimes have significant damage potential (MMI 7); significant damage effects (MMI 7) are common for **M** > 4.8 within 10 km.
4. Significant damage to structures, soil failures, and personal injuries have occurred in the epicentral region of several induced earthquakes of **M** 4.7–5.8 (e.g., Yeck *et al.*, 2017; Lee *et al.*, 2019; Lei *et al.*, 2019).
5. Hazard mitigation or avoidance measures that aim to preclude earthquake damage need to prevent the occurrence of induced earthquakes of **M** > 3.5 within ~5 km of vulnerable infrastructure.

DATA AND RESOURCES

The peak ground acceleration (PGA) and peak ground velocity (PGV) data were compiled from several sources: (1) California data are from the Next Generation Attenuation-West2 Project (NGA-W2) dataset and are taken from the study of Atkinson (2015); (2) Oklahoma data were downloaded from Incorporated Research Institutes for Seismology (IRIS), as processed and compiled by Novakovic *et al.* (2018); (3) western Canada sedimentary basin (WCSB) data were compiled from the datasets of Novakovic (2019), Mahani *et al.* (2019), and Mahani and Kao (2018). Modified Mercalli intensity (MMI) data are from the Oklahoma events studied by Atkinson *et al.* (2018), with the Oklahoma database updated to May 2019 using data obtained from the U.S. Geological Survey (USGS) "Did You Feel It?" (DYFI) archives at https://earthquake.usgs.gov/data/dyfi/ (last accessed June 2019). The DYFI data for Oklahoma events from 2010 to 2016 were obtained in April 2017, whereas the data for events from 2017 to May 2019 were obtained in May 2019. The dates when data were downloaded are provided because DYFI data are dynamic, and subject to postprocessing procedures at USGS, which may be refined over time (e.g., Wald *et al.*, 2011); such updating can lead to subtle differences in DYFI data (S. Hough, D. Wald, personal comm., 2019). The unpublished manuscript by J. Holmgren, H. Ghofrani, and G. Atkinson (2020), "Reconciling ground motions and stress drops for induced earthquakes in the western Canada sedimentary Basin," has been submitted to *Bull. Seismol. Soc. Am.*

ACKNOWLEDGMENTS

The author's research is supported by the Natural Sciences and Engineering Research Council of Canada and TransAlta. The author thanks Susan Hough, Martin Chapman, and an anonymous reviewer for constructive comments and an interesting discussion of "Did You Feel It?" (DYFI) data. The author thanks David Wald for his insights on DYFI data archival and postprocessing procedures.

REFERENCES

Allen, T. I., D. J. Wald, and C. B. Worden (2012). Intensity attenuation for active crustal regions, *J. Seismol.* **16,** 409–433.

Atkinson, G. M. (2015). Ground-motion prediction equation for small-to-moderate events at short hypocentral distances, with application to induced seismicity hazards, *Bull. Seismol. Soc. Am.* **105,** doi: 10.1785/0120140142.

Atkinson, G. M. (2017). Strategies to prevent damage to critical infrastructure from induced seismicity, *FACETS*, Science Application Forum, doi: 10.1139/facets-2017-0013.

Atkinson, G. M., and S. Kaka (2007). Relationships between felt intensity and instrumental ground motions for earthquakes in the central United States and California, *Bull. Seismol. Soc. Am.* **97,** 497–510.

Atkinson, G. M., and D. Wald (2007). "Did You Feel It?" intensity data: A surprisingly good measure of ground motion, *Seismol. Res. Lett.* **78,** 362–368.

Atkinson, G. M., D. W. Eaton, H. Ghofrani, D. Walker, B. Cheadle, R. Schultz, R. Shcherbakov, K. Tiampo, J. Gu, R. M. Harrington, *et al.* (2016). Hydraulic fracturing and seismicity in the Western Canada Sedimentary Basin, *Seismol. Res. Lett.* **87,** 631–647.

Atkinson, G. M., D. Wald, B. Worden, and V. Quitoriano (2018). The intensity signature of induced seismicity, *Bull. Seismol. Soc. Am.* **108,** doi: 10.1785/0120170316.

Atkinson, G. M., B. Worden, and D. Wald (2014). Intensity prediction equations for North America, *Bull. Seismol. Soc. Am.* **104,** 3084–3093.

Atkinson, G. M., E. Yenier, N. Sharma, and V. Convertito (2016). Constraints on the near-distance saturation of ground-motion amplitudes for small-to-moderate induced earthquakes, *Bull. Seismol. Soc. Am.* **106,** doi: 10.1785/0120160075.

Baisch, S., C. Koch, and A. Muntendam-Bos (2019). Traffic light systems: To what extent can induced seismicity be controlled?, *Seismol. Res. Lett.* **90,** doi: 10.1785/0220180337.

Boatwright, J., K. Thywissen, and L. Seekins (2001). Correlation of ground motion and intensity for the 17 January 1994 Northridge, California earthquake, *Bull. Seismol. Soc. Am.* **91,** 739–752.

Bommer, J., and J. Alarcon (2005). The prediction and use of peak ground velocity, *J. Earthq. Eng.* **10,** 1–31.

Bommer, J., A. Elnashai, and A. Weir (2000). Compatible acceleration and displacement spectra for seismic design codes, *Proc. 12th World Conf. Earthq. Eng.*, Auckland, New Zealand, 30 January–4 February 2000, Paper 0207.

Bommer, J., S. Oates, J. Mauricio Cepeda, C. Lindholm, J. Bird, R. Torres, G. Marroquin, and J. Rivas (2006). Control of hazard due to seismicity induced by a hot fractured rock geothermal project, *Eng. Geol.* **83,** 287–306.

Borcherdt, R. (1994). Estimates of site-dependent response spectra for design, *Earthq. Spectra* **10,** 617–654.

Dewey, J. W., M. G. Hopper, D. J. Wald, V. Quitoriano, and E. R. Adams (2002). Intensity distribution and isoseismal maps for the Nisqually, WA, earthquake of 28 February 2001, *U.S. Geol. Surv. Open-File Rept. 02-0346*, 57 pp.

Farrugia, J., G. Atkinson, and S. Molnar (2017). Validation of 1D earthquake site characterization methods with observed earthquake site amplification in Alberta, Canada, *Bull. Seismol. Soc. Am.* doi: 10.1785/0120170148.

Giardini, D. (2009). Geothermal quake risks must be faced, *Nature* **462,** 848–849, doi: 10.1038/462848a.

Holmgren, J., H. Ghofrani, and G. Atkinson (2019). Stress drops and directivity of induced earthquakes in the western Canada sedimentary basin, *Bull. Seismol. Soc. Am.* **109,** 635–1652.

Hough, S. (2014). Shaking from injection-induced earthquakes in the central and eastern United States, *Bull. Seismol. Soc. Am.* **104,** doi: 10.1785/0120140099.

Huang, Y., W. Ellsworth, and G. Beroza (2017). Stress drops of induced and tectonic earthquakes in the central United States are indistinguishable, *Sci. Adv.* **3,** no. 8, e1700772, doi: 10.1126/sciadv.1700772.

Joyner, W. B., and D. M. Boore (1982). Prediction of earthquake response spectra, *U.S. Geol. Surv. Open-File Rept. 82-977*, 16 pp.

Lee, K., W. Ellsworth, D. Giardini, J. Townend, S. Ge, T. Shimamoto, I. Yeo, T. Kang, J. Rhie, D. Sheen, *et al.* (2019). Managing injection-induced seismic risks, *Science* **364,** 730–732.

Lei, X., Z. Wang, and J. Su (2019). The December 2018 ML 5.7 and January 2019 ML 5.3 earthquakes in South Sichuan Basin induced by shale gas hydraulic fracturing, *Seismol. Res. Lett.* **90,** 1099–1110.

Mahani, A., and H. Kao (2018). Ground motion from M 1.5–3.8 induced earthquakes at hypocentral distance <45 km in the Montney Play of northeast British Columbia, Canada, *Seismol. Res. Lett.* **89,** 22–34.

Mahani, A., H. Kao, G. Atkinson, K. Assatourians, K. Addo, and Y. Liu (2019). Ground motion characteristics of the 30 November 2018 injection-induced earthquake sequence in northeast British Columbia, Canada, *Seismol. Res. Lett.* **90,** doi: 10.1785/0220190040.

Newmark, N. M., and W. J. Hall (1982). *Earthquake Spectra and Design*, EERI Monograph, Earthquake Engineering Research Institute, Oakland, California.

Novakovic, M. (2019). Empirical characterization of induced seismicity in Alberta and Oklahoma, *Ph.D. Thesis*, Western University, London, Canada, Electronic Thesis and Dissertation Repository 5961, available at https://ir.lib.uwo.ca/etd/5961 (last accessed December 2019).

Novakovic, M., and G. Atkinson (2015). Preliminary evaluation of ground motions from earthquakes in Alberta, *Seismol. Res. Lett.* **86,** doi: 10.1785/0220150059.

Novakovic, M., G. Atkinson, and K. Assatourians (2018). Empirically-calibrated ground-motion prediction equation for Oklahoma, *Bull. Seismol. Soc. Am.* **108,** 2444–2461.

Petersen, M., C. Mueller, M. Moschetti, S. Hoover, A. Llenos, W. Ellsworth, A. Michael, J. Rubinstein, A. McGarr, and K. Rukstales (2017). 2017 One-year seismic hazard forecast for the central and eastern United States from induced and natural earthquakes, *Seismol. Res. Lett.* doi: 10.1785/0220170005.

Rennolet, S., M. Moschetti, E. Thompson, and W. Yeck (2018). A flat-file of ground motion intensity measurements from induced earthquakes in Oklahoma and Kansas, *Earthq. Spectra* **34,** 1–20.

Rubinstein, J., and A. Mahani (2015). Myths and facts on wastewater injection, hydraulic fracturing, enhanced oil recovery, and induced seismicity, *Seismol. Res. Lett.* **86,** 1060–1067.

Seed, H. B., and I. M. Idriss (1982). *Ground Motions and Soil Liquefaction during Earthquakes*, Earthquake Engineering Research Institute Monograph, Oakland, California.

Seyhan, E., and J. Stewart (2014). Semi-empirical nonlinear site amplification from NGA-West2 data and simulations, *Earthq. Spectra* **30,** 1241–1256.

U.S. Geological Survey (1989). The severity of an earthquake, *U.S. Geol. .Surv. General Interest Publication 1989-288-913*, U.S. Geological Survey Information Services, Denver, Colorado.

Wald, D., V. Quitoriano, T. Heaton, and H. Kanamori (1999). Relationships between peak ground acceleration, peak ground velocity, and modified Mercalli intensity in California, *Earthq. Spectra* **15,** 557–564.

Wald, D. J., V. Quitoriano, C. B. Worden, M. Hopper, and J. W. Dewey (2011). USGS "Did You Feel It?" internet-based macroseismic intensity maps, *Ann. Geophys.* **54,** 688–709.

Westaway, R., and P. Younger (2014). Quantification of potential macroseismic effects of the induced seismicity that might result from hydraulic fracturing for shale gas exploitation in the UK, *Q. J. Eng. Geol. Hydrogeol.* **47,** 333–350.

White, I., T. Liu, N. Luco, and A. Liel (2017). Comparisons between the 2016 USGS induced-seismicity hazard model, "Did You Feel It?" data, and instrumental data, *Seismol. Res. Lett.* **89,** 127–137.

Worden, B., M. Gerstenberger, D. Rhoades, and D. Wald (2012). Probabilistic relationships between ground motion parameters and modified Mercalli intensity in California, *Bull. Seismol. Soc. Am.* **102,** 204–221.

Yeck, W., G. Hayes, D. McNamara, J. Rubinstein, W. Barnhart, P. Earle, and H. Benz (2017). Oklahoma experiences largest earthquake during ongoing regional wastewater injection hazard mitigation efforts, *Geophys. Res. Lett.* **44,** 711–717.

Yenier, E., and G. Atkinson (2015a). A regionally-adjustable generic GMPE based on stochastic point-source simulations, *Bull. Seismol. Soc. Am.* **105,** 1989–2009.

Yenier, E., and G. Atkinson (2015b). An equivalent point-source model for stochastic simulation of earthquake ground motions in California, *Bull. Seismol. Soc. Am.* **105,** 1435–1455.

Manuscript received 24 June 2019
Published online 10 March 2020